

Transcranial focused ultrasound modulates the activity of primary somatosensory cortex in humans

Wynn Legon¹, Tomokazu F Sato¹, Alexander Opitz^{1,2}, Jerel Mueller³, Aaron Barbour¹, Amanda Williams¹ & William J Tyler^{1,3,4}

Improved methods of noninvasively modulating human brain function are needed. Here we probed the influence of transcranial focused ultrasound (tFUS) targeted to the human primary somatosensory cortex (S1) on sensory-evoked brain activity and sensory discrimination abilities. The lateral and axial spatial resolution of the tFUS beam implemented were 4.9 mm and 18 mm, respectively. Electroencephalographic recordings showed that tFUS significantly attenuated the amplitudes of somatosensory evoked potentials elicited by median nerve stimulation. We also found that tFUS significantly modulated the spectral content of sensory-evoked brain oscillations. The changes produced by tFUS on sensory-evoked brain activity were abolished when the acoustic beam was focused 1 cm anterior or posterior to S1. Behavioral investigations showed that tFUS targeted to S1 enhanced performance on sensory discrimination tasks without affecting task attention or response bias. We conclude that tFUS can be used to focally modulate human cortical function.

Current noninvasive neuromodulation methods, such as transcranial magnetic stimulation (TMS) and transcranial direct current stimulation, offer low spatial resolutions. These methods typically produce electric fields having length scales on the order of several centimeters, which span anatomically and functionally distinct human brain circuits^{1,2}. As a result, current transcranial approaches often modulate activity not only in the intended target but also in surrounding brain circuits^{1,3}. Therefore, improved approaches to the transcranial modulation of human brain circuit activity are sought to support global brain mapping efforts, as well as to advance diagnostics and therapies in neuroscience. In the present study, we investigated the potential use of pulsed ultrasound (US) for focally modulating cortical function in humans.

Studies examining the direct effects of US on neuronal activity date back to 1929, when US was first shown to excite nerve fibers in isolated turtle and frog muscle preparations⁴. Evidence accumulated since then has shown that US can directly modulate neuronal activity in peripheral nerves^{5,6}, elicit action potentials in hippocampal slices^{7,8} and stimulate retina⁹. Further, US can noninvasively stimulate the hippocampus and motor cortex of intact mice^{10,11}, modulate

monosynaptic and polysynaptic spinal reflexes in cats¹² and disrupt seizure activity in cats¹³, rats¹⁴ and mice¹⁵. Additional evidence from animal models has demonstrated that US can elicit functional magnetic resonance imaging blood oxygen–level dependent contrast signals in the visual and motor cortices of rabbits¹⁶, reversibly suppress the amplitudes of visual evoked potentials in both cats¹⁷ and rabbits¹⁶, and functionally modulate neuronal activity in the frontal eye fields of awake, behaving monkeys¹⁸. At low intensities for short exposure times, tissue heating does not occur, so the mechanisms underlying the effects of US on neuronal activity are thought to partially stem from mechanical pressure effects of US on cellular membranes and ion channels^{5,10,16,19,20}. These mechanical actions of US have not been reported to cause tissue damage when used to modulate neuronal activity^{5,9–11,15,16,19}.

Despite observations in different animal models, it has remained untested whether US can focally modulate the activity of intact human brain circuits. Therefore, we aimed to determine whether tFUS is capable of functionally modulating brain activity in the human primary somatosensory cortex. Our findings indicate tFUS can focally modulate sensory evoked brain activity and cortical function in humans. These observations may help advance the development of enhanced noninvasive neuromodulation strategies.

RESULTS

Acoustic beam properties of tFUS

The optimal acoustic frequencies for the transcranial transmission and brain absorption of US are known to be <0.65 MHz (refs. 21,22). We used 0.5-MHz US on the basis of previous observations that it can modulate mammalian brain activity^{10,11}. First we quantified acoustic pressure fields emitted from a single-element focused ultrasound (FUS) transducer having a center frequency of 0.5 MHz, a diameter of 30 mm and a focal length of 30 mm. Using a calibrated hydrophone mounted on a motorized, three-axis stage, we recorded acoustic pressure fields transmitted from the FUS transducer into the free space of an acoustic test tank, as well as through hydrated fragments of human cranium (Fig. 1; see Online Methods). Our measurements revealed that when FUS was transmitted through the skull the spatial-peak pulse-average intensity (I_{SPPA}) dropped by approximately fourfold (1/4.05), corresponding to a –6.07 dB insertion loss with

¹Virginia Tech Carilion Research Institute, Roanoke, Virginia, USA. ²Department of Clinical Neurophysiology, Georg-August-University, Göttingen, Germany. ³School of Biomedical Engineering and Sciences, Virginia Tech, Blacksburg, Virginia, USA. ⁴Department of Psychiatry and Behavioral Medicine, Virginia Tech Carilion School of Medicine, Roanoke, Virginia, USA. Correspondence should be addressed to W.J.T. (wtyler@vt.edu).

Received 10 September 2013; accepted 4 December 2013; published online 12 January 2014; doi:10.1038/nn.3620

Figure 1 Ultrasound can be focused through human skull bone.

(a,b) Acoustic intensity fields emitted from a 0.5-MHz FUS transducer measured in free space (no skull, a) and after transcranial transmission through hydrated human cranial bone (tFUS, b). The white lines on the three-dimensional acoustic intensity maps (left) indicate the focal plane where the spatial peak pulse average intensity of the acoustic field was measured. Acoustic beam cross-sections of these focal planes are illustrated at right. (c) Line plots illustrate the lateral (x; left) and vertical (y; middle) peak normalized acoustic intensity profiles for the acoustic beam in the focal plane of 0.5-MHz FUS transmitted into free space (no skull; black) and through human cranial bone (red). Also illustrated are line plots (right) showing the axial (z) peak normalized intensity profiles of the FUS field for both the free space and transcranial conditions.

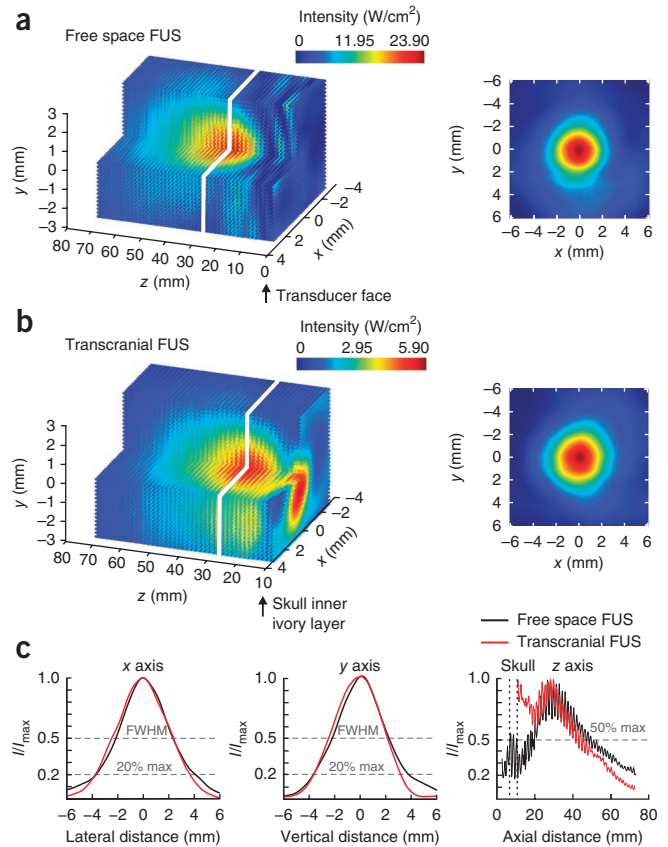
our skull sample (Fig. 1a,b). This loss varied slightly across acoustic powers (free space powers and pressures ranging from $I_{SPPA} = 0.12 \text{ W/cm}^2$ and 0.12 MPa peak-to-peak pressure to $I_{SPPA} = 50 \text{ W/cm}^2$ and 2.5 MPa peak-to-peak pressure, respectively) from a 3.7- to 4.1-fold drop in intensity when transmitting 0.5-MHz FUS through human cranial bone.

We characterized the three-dimensional shape of FUS acoustic fields in free space and after transcranial transmission (Supplementary Table 1). Transmitting FUS through human cranial bone caused an approximately 10% loss in lateral and vertical spatial resolution of the acoustic beam, estimated by the intensity full width at half maximum (FWHM; Fig. 1c). The lateral (x) and vertical (y) dimensions of FUS beam cross-sections measured at the intensity FWHM were 4.33 and 4.48 mm in the free space condition and 4.56 and 4.89 mm after transcranial transmission (Fig. 1c). We also characterized the acoustic field in the axial direction along the z axis, perpendicular to the transducer face and skull, from the spatial-peak intensity maximum to 50% and 20% maximum of intensity (Supplementary Table 1). The FUS intensity half width of the half maximum (HWHM) was 20.4 mm in the free space condition and 18.0 mm after transcranial transmission (Fig. 1c). Under these conditions, transmission of 0.5-MHz FUS through the skull led to a reduced pressure depth-of-field and an approximately 12% increase in the axial resolution. This natural focusing may be best described as a nonlinear effect that causes a cone of FUS to rotate back toward the skull insertion point, creating a more compact pressure ellipsoid-shaped acoustic field (Fig. 1c). Thus, the skull is not an obstacle for transcranial focusing of US and may actually exert an acoustic lensing effect to enhance spatial resolution under certain conditions.

Targeting tFUS to the primary sensory cortex

We targeted left S1 by transmitting tFUS beams into cortex from a transducer positioned perpendicular to the scalp at electroencephalographic (EEG) electrode site CP3 (Supplementary Fig. 1a). We visualized tFUS beam locations in the brain using realistic models of human heads generated using a finite element method (FEM). Briefly, the gray matter, white matter, cerebrospinal fluid, skin and skull were segmented from magnetic resonance images and, on the basis of the binary tissue masks, a three-dimensional FEM model of the head containing approximately 1.7 million tetrahedral elements was created (see Online Methods).

When targeting S1, the tFUS beam displayed a first prominent maximum of acoustic field strength in the brain at the top of the gyral crown in the postcentral gyrus (Fig. 2a). The tFUS field produced a second maximum of field strength in the posterior wall of the central sulcus at a depth of approximately 2 cm (Fig. 2b,c). This bimodal acoustic intensity distribution was due to the acoustic wave behavior arising from transcranial transmission, as observed during



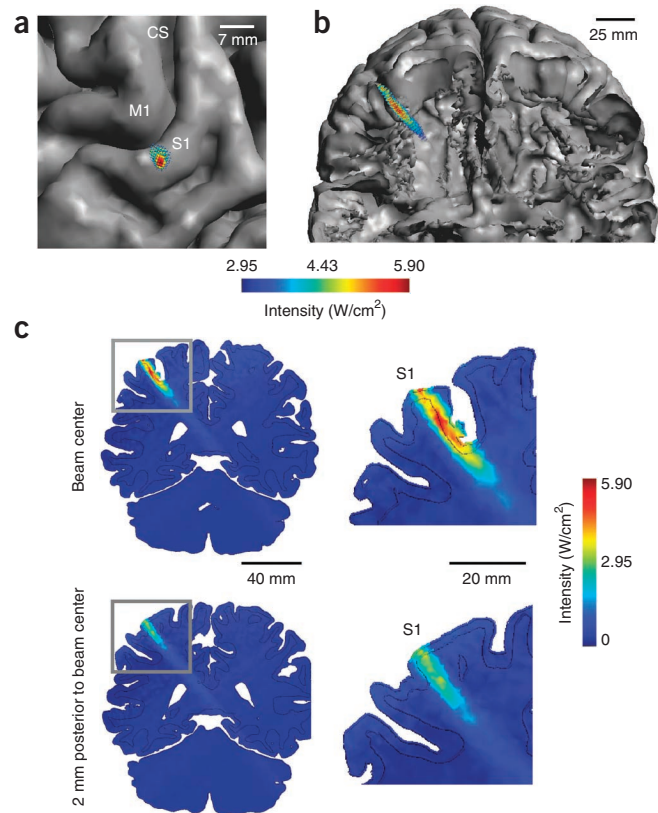
quantitative field mapping of tFUS beams (Fig. 1b,c). We observed the acoustic intensity field to drop to approximately 50% of its maximum in brain regions 2 mm anterior or posterior from the beam center (Fig. 2c).

tFUS modulates sensory-evoked brain activity

In a within-subjects design, we studied the influence of tFUS on short-latency and late-onset brain activity by examining the peak-to-peak amplitudes of somatosensory evoked potentials (SEPs) and the spectral content of evoked EEG activity elicited by right median nerve (MN) stimulation. We targeted 0.5-MHz tFUS beams to the crown and posterior wall of the left central sulcus (S1) in human participants ($N = 10$) by placing the FUS transducer at the 10-20 EEG electrode site CP3 (Supplementary Fig. 1a). EEG activity was recorded from four electrodes surrounding CP3 placed at C3, CP1, CP5 and P3. The tFUS stimulus consisted of individual pulses having a pulse duration of 360 μs repeated at 1 kHz for 500 ms. Transmission of the tFUS stimulus began 100 ms before MN stimulation (Supplementary Fig. 1b,c; see Online Methods). The sham condition was identical to the tFUS treatment except that the geometrically symmetrical inactive face (rather than the active face) of the transducer contacted the scalp to control for a chirping sound produced by the transducer during its excitation. Volunteers did not report any thermal or mechanical sensations due to tFUS transmission through the scalp. Similarly, there were no reports of perceptual differences between the sham and tFUS conditions.

The SEP produced by MN stimulation during EEG recordings has been well studied. Its components are named according to their negative (N) or positive (P) polarities and latencies (in ms) as N20, P27, N33, P50, N70, P100 and N140. The N20 component of the MN-evoked SEP has been shown to represent sensory input from the

Figure 2 tFUS can be targeted to spatially discrete regions of human cortex. (a,b) Top-down (a) and coronal cutaway view (b) showing the acoustic intensity field of the tFUS beam projected from EEG site CP3 into a realistic FEM model of the brain derived from whole-head structural magnetic resonance images. Projection of the tFUS acoustic field illustrates the targeting of primary somatosensory cortex (S1) with reference to the primary motor cortex (M1) and the central sulcus (CS). (c) Coronal magnetic resonance slices showing projections of the measured tFUS fields from EEG electrode site CP3, further illustrating the spatial specificity of 0.5-MHz tFUS in the crown of the postcentral gyrus (S1) and posterior wall of the central sulcus. Coronal slices are shown along the anterior-posterior axis of the beam corresponding to the center of the beam (top) and 2.0 mm posterior to the beam center (bottom) to show the acoustic intensity drop-off as a function of tFUS beam width.



dorsal column–medial lemniscal pathway by thalamocortical fibers originating in the ventroposterolateral nucleus of the thalamus and terminating in Brodmann area 3b (anterior bank of the postcentral gyrus facing the central sulcus) of S1 (ref. 23). Subsequent slow-onset late potentials with a latency of about 200 ms or later are thought to reflect the ensuing serial processing of somatosensory information from S1 Brodmann area 3b to areas 1 and 2, as well as to higher-level somatosensory processing areas, including posterior parietal cortex (Brodmann areas 5 and 7) and secondary somatosensory cortex, serving different functions in the encoding of stimulus representations^{24,25}.

We found that C3 most reliably captured both short-latency and late-onset brain activity evoked by MN stimulation. Compared to sham, tFUS elicited a significant reduction in the peak-to-peak amplitude of the short-latency N20–P27 SEP complex recorded at C3 (Fig. 3 and Table 1) and CP1 (sham, $1.22 \pm 0.14 \mu\text{V}$, s.e.m.; tFUS, $0.73 \pm 0.15 \mu\text{V}$; $P = 0.014$; Fig. 3). We also observed tFUS to produce a significant reduction in the amplitude of the short-latency N33–P27 SEP complex recorded at C3 (Fig. 3 and Table 1). The reduction in amplitudes of these short-latency SEP components remained stable across the duration of experiments, indicating that there were no cumulative effects of tFUS on brain activity as studied (Fig. 4). tFUS also produced significant effects on the amplitudes of the N70–P50 complex recorded at CP5 (sham, $-3.30 \pm 0.65 \mu\text{V}$; tFUS, $-2.85 \pm 0.46 \mu\text{V}$; $P = 0.017$) and P3 (sham, $-0.66 \pm 0.15 \mu\text{V}$; tFUS, $-1.42 \pm 0.23 \mu\text{V}$; $P = 0.010$) (Fig. 3). Lastly, the late potential recorded from C3 was significantly attenuated by tFUS (Fig. 3 and Table 1). In summary, we found that tFUS targeted to S1 modulated the amplitudes of both short-latency and late-onset SEP complexes.

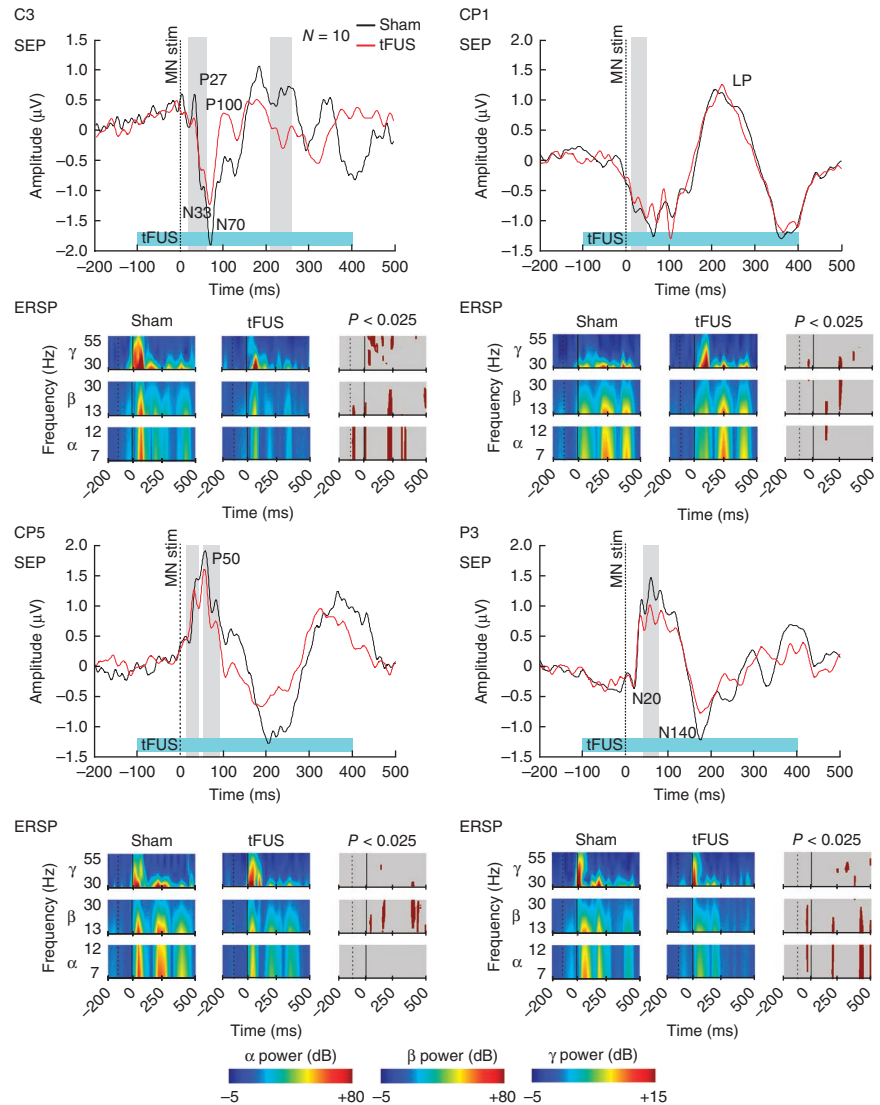
Spectral decomposition of EEG provides additional valuable information on ongoing oscillatory dynamics that is regarded as reflecting cortical excitability and information processing in the human brain^{26,27}. As such, we performed spectral decomposition on the time epoch of -200 to 500 ms around MN stimulation to further evaluate the effects of tFUS on sensory-evoked brain activity compared to sham treatment. Compared to sham, we found that tFUS significantly ($P < 0.025$) decreased the power of alpha-band (7–12 Hz) and beta-band (13–30 Hz) baseline activity recorded from EEG sites C3 and P3 in the 100 ms following the onset of tFUS transmission before MN stimulation (Fig. 3). We also found that tFUS produced a significant ($P < 0.025$) attenuation in the power of short-latency evoked gamma-band (30–55 Hz) activity occurring within 70 ms of MN stimulation (Fig. 3). As was also evident to varying degrees across the EEG channels recorded, tFUS significantly modulated the power of late-onset alpha-, beta- and gamma-band activity occurring about 200 ms after MN stimulation or later (Fig. 3).

tFUS modulates sensory detection thresholds

We next examined the behavioral effects of tFUS delivered to S1 on sensory detection thresholds using two-point and frequency discrimination tasks (see Online Methods). Briefly, participants ($N = 12$) were required to decide whether they experienced one or two stimuli in response to the application of one or two pins (spaced from 0.3 to 2.8 mm apart in 0.3 mm increments) to the pad of their right index finger for 250 ms at a constant force during sham and tFUS treatments. The presentation of sensory stimuli began 100 ms after the onset of tFUS or sham treatment. In a separate experiment on a different day, 12 subjects (10 of the subjects completed both tasks) were required to decide whether the frequency of the second of two discrete air puff trains (500 ms train duration each, 500 ms inter-stimulus interval) applied to their right index finger was higher than the frequency of the first air puff train. The frequency of the first air puff train remained constant at 100 Hz while the frequency of the second stimulus varied randomly between 100 and 150 Hz in 5-Hz increments. Sham and tFUS conditions were counterbalanced across subjects in each experiment.

Data obtained from the two-point and frequency discrimination tasks were analyzed using signal detection theory²⁸. During two-point discrimination catch trials (control trials using a single pin), the percentage of responses correct (sham, $85 \pm 5\%$; tFUS, $84 \pm 5\%$) was not different during tFUS and sham treatment ($z = 0.751$, $P = 0.453$; Supplementary Fig. 2a). These values indicate that participants' attention was directed to the task and did not differ between tFUS and sham treatments. A Wilcoxon signed-rank test revealed no difference in criterion values between the tFUS condition and the sham condition ($z = -0.756$, $P = 0.450$; Supplementary Fig. 2a). These data indicate tFUS did not affect response bias or influence participants to respond a certain way. We examined discrimination thresholds using the cumulative sensitivity index (d'), where $d' > 1$ was considered

Figure 3 tFUS targeted to human somatosensory cortex modulates sensory-evoked brain activity. Top panels, grand average ($N = 10$) SEP by electrode site (C1, CP1, CP5 and P3) as a result of right median nerve stimulation (MN stim; 100 trials) for sham (black) and tFUS (red) treatment conditions. N20, P27, N33, P50, N70, P100, N140 and late potential components of SEPs are annotated across the different electrode sites. Gray vertical bars indicate regions of significant differences ($P < 0.025$) in the peak-to-peak amplitudes of SEP complexes between sham and tFUS conditions. Bottom, time-frequency plots illustrating the spectral power of evoked brain oscillations in the alpha (7–12 Hz), beta (13–30 Hz) and gamma (30–55 Hz) frequency bands in relation to the onset of tFUS (dashed vertical line) and MN stimulation (solid vertical line) for sham and tFUS treatment conditions. Statistical difference plots are also shown for each frequency band: maroon regions indicate a significant difference ($P < 0.025$) between sham and tFUS treatment conditions. Color scale at the bottom of the figure indicates the power for each frequency band.



the discrimination threshold (Fig. 5). A Wilcoxon signed-rank test revealed that volunteers showed significant improvements in their ability to distinguish pins at closer distances during tFUS treatments compared to sham ($z = 2.196$, $P = 0.028$; Fig. 5a).

A Wilcoxon signed-rank test revealed that subjects were also significantly better at discriminating small frequency differences between successive air puff trains during tFUS trials compared to sham ($z = 2.102$, $P = 0.036$; Fig. 5b). The percentage of responses correct during randomly administered air puff frequency discrimination catch trials (where the air puff trains had equal frequencies) did not differ between tFUS and sham conditions (sham, $80 \pm 6\%$; tFUS, $83 \pm 5\%$; $z = 0.253$, $P = 0.800$; Supplementary Fig. 2b), indicating that participant attention did not differ across treatments. Likewise, tFUS did not alter participants' response bias compared to sham as indicated by a Wilcoxon signed-rank test on the criterion values obtained during frequency discrimination testing ($z = -0.203$, $P = 0.840$; Supplementary Fig. 2b). Collectively, these data show that tFUS enhanced the somatosensory discrimination abilities of participants as assessed by two-point and frequency discrimination tasks, without affecting response bias or task attention.

Table 1 Mean amplitudes of SEP complexes recorded from C3 when tFUS beam was targeted to S1

| SEP complex | Mean amplitude \pm s.e.m. (μ V) | | P value |
|----------------|--|------------------|---------|
| | Sham | tFUS | |
| P27–N20 | 0.83 \pm 0.15 | 0.38 \pm 0.09 | 0.011* |
| N33–P27 | -1.66 \pm 0.15 | -0.99 \pm 0.13 | 0.043* |
| P50–N33 | 3.12 \pm 0.50 | 2.72 \pm 0.44 | 0.244 |
| N70–P50 | -2.21 \pm 0.40 | -2.42 \pm 0.62 | 0.783 |
| P100–N70 | 1.54 \pm 0.48 | 2.66 \pm 0.85 | 0.530 |
| N140–P100 | -1.72 \pm 0.46 | -1.71 \pm 0.72 | 0.715 |
| Late potential | 3.78 \pm 0.85 | 2.87 \pm 0.85 | 0.004* |

* $P < 0.05$.

tFUS modulation of brain activity is spatially restricted

We next studied the focal specificity of tFUS by analyzing SEP complex amplitudes and the spectral content of EEG activity elicited by MN stimulation within volunteers ($N = 8$) when transducers were placed 1 cm anterior and 1 cm posterior to the CP3 location in a counterbalanced manner. Here we focused on examining the influence of tFUS on EEG activity recorded from electrode C3 because it best captured the early sensory components of SEPs as described above. With respect to targeting, our FEM models showed that moving the FUS transducer 1 cm anterior to CP3 generated an acoustic beam in brain regions located across the central sulcus in the precentral gyrus. Similarly, displacing the transducer 1 cm posterior to CP3 resulted in the acoustic beam being focused in brain regions posterior to the crown of the postcentral gyrus (Fig. 6a). This displacement of acoustic beams along the anterior-posterior axis enabled the targeting of non-overlapping and spatially discrete brain regions by tFUS.

Whereas tFUS targeted to the crown and posterior wall of the central sulcus (S1) produced a significant decrease in the amplitude of both short-latency (N20/P27 and P27/N33) and late-onset SEP complexes (Fig. 3 and Table 1), moving the acoustic beam 1 cm anterior or posterior from this site abolished these effects. Specifically, there were no significant differences between the amplitudes of any

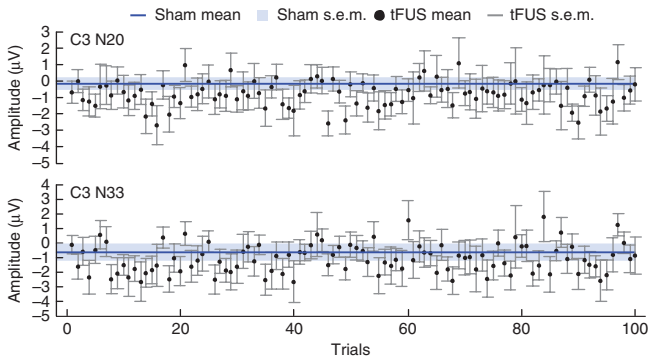


Figure 4 The influence of tFUS on brain activity is not cumulative and remains stable across time. Plots of the trial mean amplitudes for N20 and N33 components of SEPs recorded from C3 during tFUS treatment are plotted as a function of trial number. The tFUS trial data are plotted against the grand average mean \pm s.e.m. of the N20 and N33 SEP amplitudes recorded during sham treatments. There were no cumulative effects of tFUS across trial number. Error bars represent s.e.m.

SEP complexes recorded during tFUS and sham treatments when transducers were positioned 1 cm anterior or posterior to CP3 (Fig. 6b and Supplementary Tables 2 and 3). Spectral decomposition further confirmed this observation, as moving the transducer either to the anterior or posterior position yielded similar spectral profiles across tFUS and sham treatments (Fig. 6b). These similar spectral patterns are in contrast to our observations that tFUS targeted to S1 produced significant effects on the power of specific brain wave activity patterns. For example, when the acoustic beam

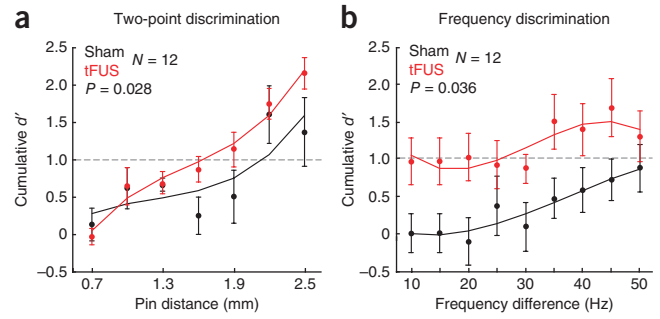


Figure 5 tFUS targeted to somatosensory cortex enhances sensory discrimination abilities in humans. (a) Data acquired under sham (black) and tFUS (red) treatments during two-point discrimination testing. The group average ($N = 12$) cumulative d' data show that the pin distance needed to achieve a threshold d' of 1 was lower for tFUS than for sham. (b) Data acquired under sham (black) and tFUS (red) treatments during frequency discrimination testing. The group average ($N = 12$) cumulative d' data show that the frequency separation to achieve a threshold d' prime of 1 was lower for tFUS treatment than for sham. Data from these psychophysical studies show that tFUS treatment significantly lowered sensory discrimination thresholds without affecting task attention or decision bias (see Supplementary Fig. 2). Error bars represent s.e.m.

was targeted to S1, we observed that tFUS significantly decreased the power of short-latency gamma-band activity occurring within 70 ms of MN stimulation (Fig. 3). When the acoustic field was focused 1 cm anterior or posterior to the postcentral gyrus, however, tFUS failed to produce a significant effect on short-latency evoked gamma activity (Fig. 6b).

Curiously, when the acoustic beam was targeted to the precentral gyrus (1 cm anterior of CP3) tFUS significantly increased the power of late-onset gamma-band activity occurring around 300 ms after MN stimulation (Fig. 6b). These results indicate that

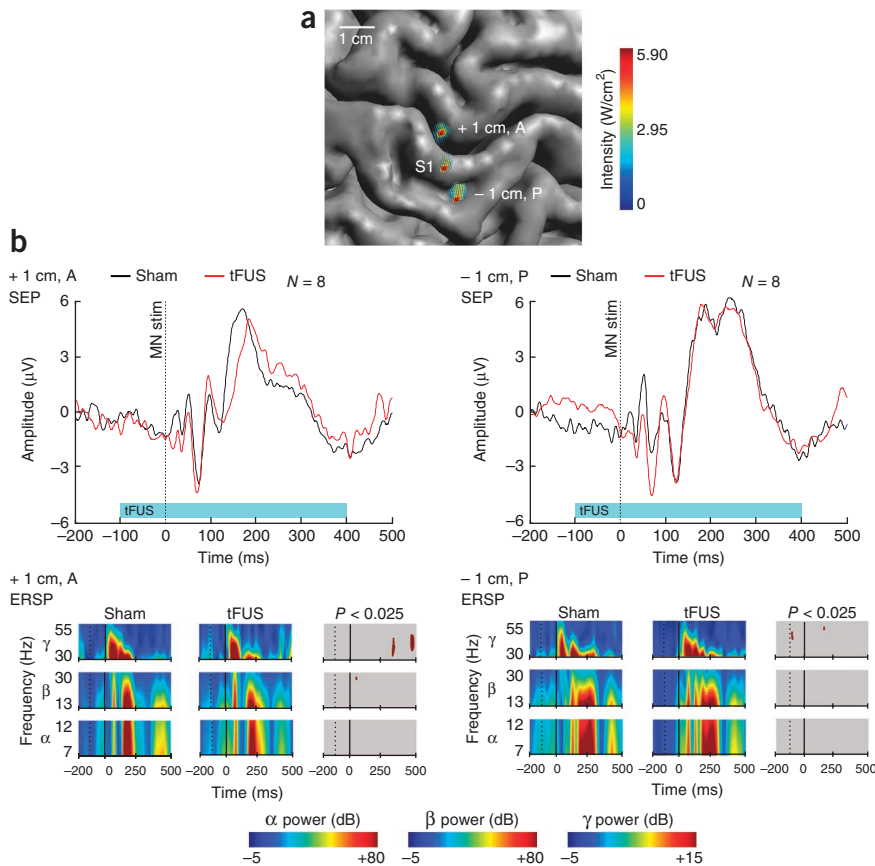


Figure 6 tFUS produces differential effects on sensory-evoked activity as a function of the brain region targeted. (a) Top-down view of the brain shows the spatial location of tFUS beams targeting the crown of the post-central gyrus (S1) and sites 1 cm anterior (+ 1 cm, A) and posterior (- 1 cm, P). (b) Top, SEP traces recorded from electrode C3 showing the grand average ($N = 8$) responses to right median nerve stimulation (MN stim; 100 trials) for sham (black) and tFUS (red) at 1 cm anterior (left) or 1 cm posterior (right) to S1. There were no significant peak-to-peak amplitude differences between sham and tFUS conditions when transducers were offset 1 cm from S1. Bottom, time-frequency plots illustrating the power of evoked brain oscillations in the alpha (7–12 Hz), beta (13–30 Hz) and gamma (30–55 Hz) frequency bands in relation to the onset of tFUS (dashed vertical line) and MN stimulation (solid vertical line) for sham and tFUS treatment conditions. Statistical difference plots are also shown for each frequency band: maroon regions indicate a significant difference ($P < 0.025$) between sham and tFUS conditions. Color scales indicate the power for each frequency band.

tFUS differentially affected short-latency evoked gamma activity, as well as late-onset induced gamma activity, as a function of the anatomical region targeted by the acoustic beam. Considering these anatomical and neurophysiological observations, we are led to conclude tFUS can modulate human cortical function while conferring a high spatial resolution in modular areas of cortex separated by about 1 cm or less. This spatial resolution of tFUS is better than those conferred by conventionally applied TMS or transcranial direct current stimulation (tDCS).

DISCUSSION

Using a single-element focused transducer, we show that 0.5-MHz US can be focused through human skull to produce acoustic beam profiles having a lateral spatial resolution of approximately 4.9 mm and an axial spatial resolution of about 18.0 mm from the focal distance. Our electrophysiological observations demonstrated that tFUS beams targeted to S1 could focally modulate short-latency and late-onset evoked cortical activity elicited in humans by somatosensory (median nerve) stimulation. Behavioral investigations revealed that tFUS targeted to S1 enhanced the somatosensory discrimination abilities of volunteers. Collectively, these observations demonstrate the utility of tFUS in the noninvasive modulation of human cortical function.

Targeting the spatiotemporal effects of tFUS

In the present study we implemented a sham condition, which controlled, as described above, for sounds made by the transducer when it was active. Subjects reported that the chirping sounds during sham and tFUS treatments were indistinguishable from one another. Further, they did not report any sensations specific to FUS transmission through their skin or skull. In contrast, however, we have previously shown that distinct US waveforms applied to the skin of the periphery can induce tactile and thermal sensations and differentially trigger brain activity patterns in sensory circuits²⁹. Thus, it is important to distinguish several features of the tFUS waveform used in the present study from US waveforms we have previously used to stimulate the somatosensory periphery²⁹.

The pulse duration (360 μ s) of the tFUS waveform used in the present study was too short and the pulse repetition frequency (1 kHz) too high to activate somatosensory receptors and fibers²⁹. Through 64-channel EEG recordings, functional magnetic resonance imaging and subjective reports, we have previously shown that US waveforms must be tuned for the activation of specific somatosensory receptors or fibers located in human skin²⁹. For example, in our previous studies we showed that low pulse repetition frequencies (10–70 Hz) and long pulse durations (7–10 ms) elicit vibratory or buzzing sensations transduced by skin receptors or mechanosensory fibers²⁹. We also showed that thermal sensations can be elicited when delivering continuous wave US (100% duty cycle) to the skin for at least 1 s (ref. 29). It is therefore critical to recognize that US waveforms having different spatial peak and temporal average energy profiles can exert unique effects on a variety of cellular populations and neuronal structures^{11,15,30,31}. The US waveform used in the present study was chosen partially for its inability to produce mechanical or thermal sensory effects on the skin or scalp.

In the present study we transmitted tFUS beams to the crown of the postcentral gyrus (S1) and posterior wall of the central sulcus. The projection of the acoustic beam path is consistent with our physiological observations that tFUS significantly affected the amplitudes of short-latency SEP complexes. This claim is supported by the fact that the short-latency SEP components in monkeys and humans are

generated in S1 Brodmann areas 3b and 1 on the posterior wall of the central sulcus and crown of the postcentral gyrus^{23,32}. When targeted to brain regions 1 cm posterior or 1 cm anterior to the postcentral gyrus, the effects of tFUS on evoked brain activity elicited by MN stimulation were abolished. In contrast, we have found that moving TMS coils in 1 cm or greater increments from a motor hotspot may not be sufficient to produce significant changes in the amplitudes of motor evoked potentials³³. Our observations here show that the influence of tFUS on brain activity can be restricted to discrete modules of cortex located within 1 cm of each other. It is not yet known, however, whether US exerts its effects primarily on dendrites, axons or cell bodies of neurons. It will be important for future studies to examine these potential cellular sites of action, as tFUS may exert specific effects on anatomically distinct regions of the neuropil.

The temporal dynamics of US-induced changes in brain activity have been shown to have delayed onset kinetics when compared to those observed with other stimulation modalities, such as electrical stimulation¹⁰. In the present study, tFUS produced an effect on baseline alpha- and beta-band activity within 20 ms of US waveform transmission. This time course for the emergence of direct US-induced effects on baseline brain activity is consistent with previous electrophysiological and imaging observations made in rodents^{10,11,15} and rabbits¹⁶. In the present study we aimed to determine whether tFUS could be used for targeted cortical modulation in humans by monitoring its influence on sensory-evoked brain activity. On the basis of the stability of SEP amplitudes recorded across tFUS trials, we conclude that there were no cumulative effects of tFUS on brain activity as studied here. Rather, we found the acute effects of tFUS on brain activity to be short-lived (<1 s). Both shorter and longer lasting effects of US on brain activity have been described, depending on numerous factors, including the US waveform characteristics implemented, as well as the anatomical and physiological features of the brain region targeted^{10,11,14–16}. In chronic pain sufferers, for example, a transcranial US waveform (8 MHz for 15 s) transmitted through the temporal window to the human posterior frontal cortex leads to a reduction in pain ratings and improved mood for up to 40 min (ref. 34). Unraveling the spatial and temporal complexities underlying the ability of US to modulate brain activity will require further efforts.

Safety of tFUS

Ultrasound has not caused tissue damage in studies implementing its nonthermal bioeffects to modulate neuronal activity at acoustic intensities below those recommended for safe use in diagnostic imaging^{5,9–11,15,16}. However, appropriate precautions and procedures must be followed to ensure the safe use of US for modulating human brain activity. To avoid the generation of standing waves, we followed the recommendations of O'Reilly *et al.*³⁵ and used a broadband, sharply focused US transducer operating in a pulsed wave mode. Others have also shown that the rate of tissue (cranium, skin and soft tissue) heating is slower and the likelihood of transient cavitation is reduced when using pulsed waves versus continuous wave US^{35–39}.

With respect to acoustic power, the I_{SPPA} of the tFUS waveform we used (23.87 W/cm²) was below the 190 W/cm² maximum recommended limit for diagnostic imaging applications^{36–38}. We also used short duration (500 ms) tFUS waveforms as stimuli, as this is not enough exposure time for relatively low-intensity pulsed US to produce appreciable tissue heating. Ultrasound at high intensities or during long exposures can cause irreversible tissue damage, like any energy source, so caution should be used when implementing it to modulate brain activity.

Physiological mechanisms underlying the effects of tFUS

Given the influence of tFUS on sensory-evoked brain activity, we naturally questioned whether it could affect sensory discrimination behavior. The psychological and neurobiological mechanisms underlying simple decisions⁴⁰ and sensory discrimination behaviors⁴¹ are complex. Not surprisingly, it is therefore difficult to relate sensory evoked physiology to stimulus discrimination behaviors. In the present study we found that tFUS enhanced sensory discrimination performance on two-point and frequency discrimination tasks without altering task attention or decision bias. This improvement of sensory discrimination behaviors under tFUS treatment conditions may seem paradoxical, as tFUS produced a reduction in the amplitude of SEP complexes, but several mechanistic possibilities exist that can explain these observations.

The focal volume of the ellipsoid acoustic beam we implemented was approximately 0.21 cm³ at half maximum field intensity. Within this volume the 500-ms pulsed acoustic pressure wave may locally shift the balance of excitation and inhibition by acting on mechanically sensitive components of the brain, including cell membranes, ion channels and synaptic vesicle cycles⁴². Our physiological observations suggest that tFUS transiently shifts the balance of neuronal activity in favor of local inhibition. Short-latency evoked gamma activity has been related to the N20 component of MN-elicited SEPs and is thought to represent cortical activity responsible for the initial encoding of a sensory stimulus^{43,44}. Thus, one hypothesis consistent with the reduction of short-latency evoked gamma activity we observed during tFUS treatment is that the pulsed acoustic pressure waves dampen excitation or increase local interneuron firing and perhaps modulate the activity of fast-spiking interneurons. Stated differently, the same amount of incoming sensory activity from a MN stimulus could be acting on populations of neurons, which are under the influence of increased local inhibition triggered by tFUS.

As described above, the rendering of cortex less sensitive to sensory-encoding thalamocortical activity explains the reduction in SEP amplitudes we observed during tFUS treatment. Increased local inhibition produced by tFUS might serve as a filter by reducing the spatial spread of cortical excitation in response to MN stimulation or during sensory discrimination tasks. Such actions could theoretically result in more spatially restricted population activation patterns, thereby yielding improvements in the cortical representation of tactile stimuli. This hypothesis helps to explain the enhancement of somatosensory discrimination we observed in response to tFUS treatment. Several other mechanistic explanations certainly exist, so it is difficult to draw any definitive conclusions. Gaining a better understanding of how pulsed US affects the balance of inhibition and excitation in targeted brain regions, as well as how it influences the activity of local circuits versus long-range connections, will advance our ability to apply tFUS to the study and mapping of human brain circuits.

tFUS for functional brain mapping

One of the most enticing applications of tFUS is its emerging utility for noninvasive, functional brain mapping in humans. Here tFUS provides a highly focused energy source capable of noninvasively producing changes in human brain activity. In neurosurgical applications, transcranial high-intensity focused ultrasound (HIFU) was recently combined with magnetic resonance thermometry to heat and destroy the ventral intermediate nucleus of the thalamus for the successful treatment of essential tremor in awake, behaving patients⁴⁵. During magnetic resonance-guided stereotactic targeting of HIFU beams (MRgHIFU), Elias *et al.*⁴⁵ observed that subablative heating of ventroposterolateral thalamic regions induced sensory effects, such as

paresthesia of the lips and fingers, in some patients. However, subablative sonication events targeting the ventral intermediate region of the thalamus produced transient suppression of postural tremor, thereby providing a functional confirmation of the ablation target before lesioning with HIFU⁴⁵. This functional mapping of deep-brain nuclei in humans with transcranial MRgHIFU enabled the active refinement of lesion coordinates such that ablation of the ventral intermediate nuclei could be achieved without destroying adjacent sensory regions of the thalamus.

The neuromodulation produced by MRgHIFU was elicited by focally heating deep-brain nuclei to around 48 °C for about 10 s during transcranial transmission of 0.65-MHz continuous-wave US at intensities <550 W/cm² from 1,024 transducers operating in a phased array⁴⁵. In the present report, we describe an approach where lower intensity US (23.87 W/cm²) transmitted from a single-element 0.5-MHz FUS transducer for 500 ms can be used to transiently modulate brain activity in the cortex of humans. Taken together, these observations highlight the potential of using tFUS for modulating and mapping brain function in both laboratory and clinical settings. Further studies are needed to validate and refine the thermal and nonthermal neuromodulation potential of tFUS. These rapidly evolving capabilities of tFUS should encourage changes in the way we study human brain function and support the exploration of new approaches to treating brain disorders. Thus, we anticipate many advances for neuroscience when extending the capabilities of tFUS for noninvasively modulating human brain circuits.

METHODS

Methods and any associated references are available in the [online version of the paper](#).

Note: Any Supplementary Information and Source Data files are available in the online version of the paper.

ACKNOWLEDGMENTS

Funding and equipment for this study was provided by a Technological Innovation Award from the McKnight Endowment for Neuroscience, Neurotek, Inc. and the Virginia Tech Carilion Research Institute.

AUTHOR CONTRIBUTIONS

W.L., T.F.S., A.O., J.M., A.B., A.W. and W.J.T. performed the experiments; W.L., T.F.S., A.O. and W.J.T. wrote the manuscript; W.L., T.F.S., A.O. and W.J.T. conducted the data analyses; W.J.T. supervised the project.

COMPETING FINANCIAL INTERESTS

The authors declare competing financial interests: details are available in the [online version of the paper](#).

Reprints and permissions information is available online at <http://www.nature.com/reprints/index.html>.

1. Thielscher, A., Opitz, A. & Windhoff, M. Impact of the gyral geometry on the electric field induced by transcranial magnetic stimulation. *Neuroimage* **54**, 234–243 (2011).
2. Opitz, A. *et al.* How the brain tissue shapes the electric field induced by transcranial magnetic stimulation. *Neuroimage* **58**, 849–859 (2011).
3. Thielscher, A. & Kammer, T. Electric field properties of two commercial figure-8 coils in TMS: calculation of focality and efficiency. *Clin. Neurophysiol.* **115**, 1697–1708 (2004).
4. Harvey, E.N. The effect of high frequency sound waves on heart muscle and other irritable tissues. *Am. J. Physiol.* **91**, 284–290 (1929).
5. Mihran, R.T., Barnes, F.S. & Wachtel, H. Temporally-specific modification of myelinated axon excitability in vitro following a single ultrasound pulse. *Ultrasound Med. Biol.* **16**, 297–309 (1990).
6. Tsui, P.H., Wang, S.H. & Huang, C.C. In vitro effects of ultrasound with different energies on the conduction properties of neural tissue. *Ultrasonics* **43**, 560–565 (2005).
7. Tyler, W.J. *et al.* Remote excitation of neuronal circuits using low-intensity, low-frequency ultrasound. *PLoS ONE* **3**, e3511 (2008).

8. Bachtold, M.R., Rinaldi, P.C., Jones, J.P., Reines, F. & Price, L.R. Focused ultrasound modifications of neural circuit activity in a mammalian brain. *Ultrasound Med. Biol.* **24**, 557–565 (1998).
9. Menz, M.D., Oralkan, O., Khuri-Yakub, P.T. & Baccus, S.A. Precise neural stimulation in the retina using focused ultrasound. *J. Neurosci.* **33**, 4550–4560 (2013).
10. Tufail, Y. *et al.* Transcranial pulsed ultrasound stimulates intact brain circuits. *Neuron* **66**, 681–694 (2010).
11. King, R.L., Brown, J.R., Newsome, W.T. & Pauly, K.B. Effective parameters for ultrasound-induced in vivo neurostimulation. *Ultrasound Med. Biol.* **39**, 312–331 (2013).
12. Shealy, C.N. & Henneman, E. Reversible effects of ultrasound on spinal reflexes. *Arch. Neurol.* **6**, 374–386 (1962).
13. Manlapaz, J.S., Astroem, K.E., Ballantine, H.T. Jr. & Lele, P.P. Effects of ultrasonic radiation in experimental focal epilepsy in the cat. *Exp. Neurol.* **10**, 345–356 (1964).
14. Min, B.K. *et al.* Focused ultrasound-mediated suppression of chemically-induced acute epileptic EEG activity. *BMC Neurosci.* **12**, 23 (2011).
15. Tufail, Y., Yoshihiro, A., Pati, S., Tauchmann, M.L. & Tyler, W.J. Ultrasonic neuromodulation by brain stimulation with transcranial ultrasound. *Nat. Protoc.* **6**, 1453–1470 (2011).
16. Yoo, S.S. *et al.* Focused ultrasound modulates region-specific brain activity. *Neuroimage* **56**, 1267–1275 (2011).
17. Fry, F.J., Ades, H.W. & Fry, W.J. Production of reversible changes in the central nervous system by ultrasound. *Science* **127**, 83–84 (1958).
18. Deffieux, T. *et al.* Low-intensity focused ultrasound modulates monkey visuomotor behavior. *Curr. Biol.* **23**, 2430–2433 (2013).
19. Krasovitski, B., Frenkel, V., Shoham, S. & Kimmel, E. Intramembrane cavitation as a unifying mechanism for ultrasound-induced bioeffects. *Proc. Natl. Acad. Sci. USA* **108**, 3258–3263 (2011).
20. Tyler, W.J. Noninvasive neuromodulation with ultrasound? A continuum mechanics hypothesis. *Neuroscientist* **17**, 25–36 (2011).
21. White, P.J., Clement, G.T. & Hynynen, K. Local frequency dependence in transcranial ultrasound transmission. *Phys. Med. Biol.* **51**, 2293–2305 (2006).
22. Hayner, M. & Hynynen, K. Numerical analysis of ultrasonic transmission and absorption of oblique plane waves through the human skull. *J. Acoust. Soc. Am.* **110**, 3319–3330 (2001).
23. Allison, T. *et al.* Human cortical potentials evoked by stimulation of the median nerve. I. Cytoarchitectonic areas generating short-latency activity. *J. Neurophysiol.* **62**, 694–710 (1989).
24. Hari, R. & Forss, N. Magnetoencephalography in the study of human somatosensory cortical processing. *Phil. Trans. R. Soc. Lond. B* **354**, 1145–1154 (1999).
25. Burton, H. & Sinclair, R.J. Attending to and remembering tactile stimuli: a review of brain imaging data and single-neuron responses. *J. Clin. Neurophysiol.* **17**, 575–591 (2000).
26. Buzsáki, G. & Draguhn, A. Neuronal oscillations in cortical networks. *Science* **304**, 1926–1929 (2004).
27. Makeig, S., Debener, S., Onton, J. & Delorme, A. Mining event-related brain dynamics. *Trends Cogn. Sci.* **8**, 204–210 (2004).
28. Swets, J.A. Is there a sensory threshold? *Science* **134**, 168–177 (1961).
29. Legon, W., Rowlands, A., Opitz, A., Sato, T.F. & Tyler, W.J. Pulsed ultrasound differentially stimulates somatosensory circuits in humans as indicated by EEG and fMRI. *PLoS ONE* **7**, e51177 (2012).
30. Gavrilov, L.R., Tsurulnikov, E.M. & Davies, I.A. Application of focused ultrasound for the stimulation of neural structures. *Ultrasound Med. Biol.* **22**, 179–192 (1996).
31. Bystritsky, A. *et al.* A review of low-intensity focused ultrasound pulsation. *Brain Stimul.* **4**, 125–136 (2011).
32. Allison, T., Wood, C.C., McCarthy, G. & Spencer, D.D. Cortical somatosensory evoked potentials. II. Effects of excision of somatosensory or motor cortex in humans and monkeys. *J. Neurophysiol.* **66**, 64–82 (1991).
33. Opitz, A. *et al.* Physiological observations validate finite element models for estimating subject-specific electric field distributions induced by transcranial magnetic stimulation of the human motor cortex. *Neuroimage* **81**, 253–264 (2013).
34. Hameroff, S. *et al.* Transcranial ultrasound (TUS) effects on mental states: a pilot study. *Brain Stimul.* **6**, 409–415 (2013).
35. O'Reilly, M.A., Huang, Y. & Hynynen, K. The impact of standing wave effects on transcranial focused ultrasound disruption of the blood-brain barrier in a rat model. *Phys. Med. Biol.* **55**, 5251–5267 (2010).
36. O'Brien, W.D. Jr. Ultrasound-biophysics mechanisms. *Prog. Biophys. Mol. Biol.* **93**, 212–255 (2007).
37. Nyborg, W.L. Biological effects of ultrasound: development of safety guidelines. Part II: general review. *Ultrasound Med. Biol.* **27**, 301–333 (2001).
38. Dalecki, D. Mechanical bioeffects of ultrasound. *Annu. Rev. Biomed. Eng.* **6**, 229–248 (2004).
39. Leighton, T.G. What is ultrasound? *Prog. Biophys. Mol. Biol.* **93**, 3–83 (2007).
40. Smith, P.L. & Ratcliff, R. Psychology and neurobiology of simple decisions. *Trends Neurosci.* **27**, 161–168 (2004).
41. Romo, R. & Salinas, E. Flutter discrimination: neural codes, perception, memory and decision making. *Nat. Rev. Neurosci.* **4**, 203–218 (2003).
42. Tyler, W.J. The mechanobiology of brain function. *Nat. Rev. Neurosci.* **13**, 867–878 (2012).
43. Fukuda, M. *et al.* Short-latency median-nerve somatosensory-evoked potentials and induced gamma-oscillations in humans. *Brain* **131**, 1793–1805 (2008).
44. Tallon-Baudry, C. & Bertrand, O. Oscillatory gamma activity in humans and its role in object representation. *Trends Cogn. Sci.* **3**, 151–162 (1999).
45. Elias, W.J. *et al.* A pilot study of focused ultrasound thalamotomy for essential tremor. *N. Engl. J. Med.* **369**, 640–648 (2013).

ONLINE METHODS

Quantitative acoustic field mapping. We measured the acoustic intensity profile of the waveform using a calibrated hydrophone (HNR-0500, Onda Corporation, Sunnyvale, CA) whose signal was amplified by an AH-1100 preamplifier (Onda Corporation). The hydrophone, US transducer and skull fragment were positioned within a 58-l acrylic water tank. The hydrophone was mounted on a three-axis stage (LTS300, Thorlabs Inc, Newton, NJ) using an assortment of optomechanical components (Edmund Optics Inc., Barrington, NJ and Thorlabs Inc., Newton, NJ). The US transducer and skull fragment were positioned similarly. Custom software written in LabVIEW (National Instruments, Austin, TX) was used to control the three-axis stage as well as the timing of transducer excitation and recording of the corresponding waveform as measured by the hydrophone. Acoustic field scans were performed at 400 μm (2 to 122 mm from transducer in a 10.4 mm \times 10.4 mm region) and 200 μm (2 to 72 mm from transducer in a 5.6 mm \times 5.6 mm region). For finding the final focal plane as well as the spatial peak location, the field maps, obtained from the earlier scans were used as locators for conducting 100- μm -resolution scans. Scans around the axis (z axis) were first performed to find the focal distance; next, a 12 mm \times 12 mm scan was performed at this distance to obtain an x - y acoustic power map at the focal plane. Scans were first performed without the skull between the transducer and hydrophone. Subsequently, to test the effects of a human skull on FUS fields, we inserted a 6-mm-thick fragment of human cortical bone (rehydrated for 48 h) between the transducer and the hydrophone and repeated our scans using the same procedures, except that the starting distance to the transducer was increased to 10 mm to avoid collision between the skull and hydrophone.

Projection of tFUS fields into a realistic head model. A realistic head FEM model was created using SimNibs⁴⁶. Briefly, gray matter, white matter, CSF, skin and skull were segmented from the magnetic resonance images and, on the basis of the binary tissue masks, a three-dimensional FEM model of the head was created containing approximately 1.7 million tetrahedral elements, with higher resolution inside white matter and gray matter. To estimate the acoustic field distribution in the brain during US stimulation, the measured tFUS field (Fig. 2b) was projected into the brain assuming that the face of the transducer was placed tangential to the scalp over CP3, as in our EEG experiments described below. The density of brain was specified as 1,030 kg/m³ and the speed of sound was 1,550 m/s (ref. 47). Acoustic intensity in the mesh nodes was computed using a nearest-neighbor interpolation. It was assumed that the acoustic properties of gray matter, white matter and CSF were similar enough that effects due to impedance mismatch at the tissue interfaces were negligible.

tFUS waveform. Transcranial ultrasonic neuromodulation waveforms were generated using a two-channel, 2-MHz function generator (BK Precision Instruments) as previously described^{48,49}. Briefly, channel 1 was set to deliver US at a pulse repetition frequency (PRF) of 1.0 kHz and channel 2 was set to drive the transducer at a 0.5 MHz acoustic frequency (A_f) in a bursting mode, with channel 1 serving as an external trigger for channel 2. The pulse duration (PD) of the waveform was set to 0.36 ms by adjusting the number of cycles per pulse (c/p) on channel 2 to 180, and the stimulus duration (0.5 s) was set by adjusting the number of pulses (np) on channel 1 to 500. The output of channel 2 was sent through a 40-W linear RF amplifier (E&I 240L; Electronics & Innovation) before being sent to a custom-designed focused ultrasound transducer (Blatek, Inc., State College, PA) having a center frequency of 0.5 MHz, a diameter of 30 mm and a focal length of 30 mm. The waveform employed for tFUS stimulation had the following parameters: $A_f = 0.50$ MHz, PD = 360 μs , PRF = 1.0 kHz and $np = 500$. This produced a stimulus duration of 0.5 s yielding a peak rarefactional pressure of 0.80 MPa, a mechanical index of 1.13 and a spatial-peak pulse-average intensity (I_{SPPA}) of 23.87 W/cm² before transcutaneous and transcranial transmission. We have previously verified this waveform does not produce heating of the skin or skull bone. The transducer was coated with acoustic coupling gel and placed on the scalp at the 10–20 electrode location CP3 before being secured in place with athletic prewrap bandaging.

Characterizing the effects of tFUS on sensory-evoked brain activity. *Participants.* The Institutional Review Board at Virginia Tech approved all

experimental procedures. Ten volunteer study participants (5 male, 5 female, aged 18–47 with a mean age of 27.0 ± 9.5 years) provided written informed consent to participate in the study. None of the volunteers reported any neurological impairment and were all self-reported as right-hand dominant.

Experimental setup. Participants were seated in a high-back desk chair with their right forearm fully supported in supination. During testing, subjects were required to sit passively while viewing a fixation cross on a screen. A total of 120 ultrasonic waveforms (see below) were delivered from the 10–20 EEG electrode site CP3 at an inter-stimulus interval (ISI) of 6 s with a positive randomization of 4 s. The tFUS treatment condition involved acoustically coupling the active face of the ultrasound transducer to the scalp at EEG site CP3 using ultrasound gel. The sham condition involved having the US transducer coupled to the head at CP3, but flipped upside down such that the inactive face of the transducer (symmetrical to the active face) made contact with the scalp but ultrasonic energy was not transmitted into the head. This approach was used to account for a chirping sound when the transducer was active. This chirping sound was identical for both the sham and tFUS conditions, and no subjects reported any sensory or perceptual differences between the two conditions. The order of sham or tFUS treatment was randomized for each subject. Total collection time was approximately 1 h.

Electroencephalography. Electroencephalography (EEG) data were acquired using a DC amplifier (BrainAmp MR Plus, Brain Products GmbH, Gilching, Germany) with four 10-mm gold-over-silver cup electrodes placed at electrodes sites C1, CP1, CP5 and P3 referenced to the left mastoid and grounded to the left ulnar styloid process. Cup electrodes were filled with a conductive paste (Ten20 Conductive; Weaver and Company, Aurora, CO) and held in place with tape. The scalp was first prepared with a mild abrasive gel (Nuprep; Weaver and Company, Aurora, CO) and rubbing alcohol. Electrode impedances were verified (<5 k Ω) before recording. EEG data were on-line filtered (DC–200 Hz) and digitized at 1,000 Hz before being stored on a computer for subsequent off-line analysis. Somatosensory evoked potentials (SEPs) were elicited in response to right median nerve stimulation using a 0.2-ms square-wave pulse driven by an SD-9 stimulator (Grass Technologies, Warwick, RI) delivered through a bar electrode (2 cm electrode spacing) affixed to the wrist. Intensity was adjusted to elicit a slight twitch of the thumb. Stimuli were delivered at an inter-stimulus interval of 6 s with a 4-s positive randomization. In each treatment condition, a total of 120 MN stimuli were delivered, of which, owing to artifact rejection in analyses, 100 random EEG responses to stimuli were used. Median nerve stimuli were time-locked to occur 100 ms after the onset of tFUS waveforms (Supplementary Fig. 1b). The experimenters conducting experiments were not blinded to the experimental condition, but the researcher processing and analyzing the acquired EEG data was.

Statistical analysis of somatosensory evoked potentials. EEG data were pre-processed using EEGLAB v12.0.0.0b⁵⁰ and Matlab v7.10.0 (The MathWorks, Inc., Natick, MA). Data were band-pass filtered (2–90 Hz) and notch filtered (60 Hz). Data were epoched around median nerve stimulus (–200 to 500 ms) and baseline corrected (–200 to –100 ms). Data were inspected for artifacts using automatic rejection criteria of an absolute peak-to-peak amplitude of 75 μV and 60 $\mu\text{V}/\text{ms}$. Waveform peak amplitude and latency were identified and quantified using custom software written in LabVIEW (National Instruments, Austin, TX, USA). All classically defined SEP components were assessed. This included the N20, P27, N33, P50, N70, P100, N140 and late potential (LP). The LP was defined as the positive (CP1 and C3) or negative (CP5 and P3) potential with a latency in the 200 ms range (Fig. 3). A distinct inflection of the waveform was necessary for inclusion in statistical analyses. Statistical analyses were performed on mean peak-to-peak amplitudes for the N20/P27, N33/P27, P50/N33, N70/P50, P100/N70, N140/P100 and LP components of SEPs recorded during sham and tFUS treatment conditions ($n = 10$ subjects, 100 trials each for each condition). To statistically analyze these SEP components recorded from multiple electrodes and at different time regions of interest, we used nonparametric permutation statistics, which appropriately control for multiple comparisons problems encountered in analyses of complex EEG data sets⁵¹. Randomization tests were conducted similarly to those described in ref. 51, where statistical P values represent the proportion of 1,000 random partitions resulting in a test statistic larger than the t value calculated by a conventional paired t -test (two-tailed, d.f. = 9) on the data.

$P < 0.025$ was considered statistically significant. Values for SEP amplitudes are reported as mean \pm s.e.m.

To assess the immediacy and stability of the effects exerted by tFUS on the amplitudes of SEP potentials, we quantified data for individual trials for each subject for both tFUS and sham conditions. Because we were unable to reliably detect SEP peaks from individual trials, amplitude was quantified from set time windows centered on peak latency of each potential of interest (i.e., N20 = 20 ms) with a time envelope approximated to the full-width half maximum of the potential of interest rounded to the nearest millisecond quantified from the grand average ($n = 10$) trace recorded from electrode site C3. Thus, for example, N20 amplitude for each trial was taken as the average from time points 18 to 22 ms. Data points from each time window were averaged to create a single value for each potential of interest for each trial. These data were averaged across each subject ($n = 10$) and are presented as mean \pm s.e.m. for both tFUS and sham condition.

Statistical analysis spectral content. We conducted spectral analysis using Matlab v7.10.0 (The MathWorks, Inc., Natick, MA). Spectral decomposition measures average dynamic changes in amplitude of a broadband EEG frequency spectrum as a function of time relative to an experimental event⁵². Spectral content was calculated using a short-time Fourier transform with a window size of 50 ms and a 25 ms overlap. Each segment was windowed with a Hamming window. The color of each pixel in the generated spectral image then indicates the power (dB) at a given frequency and latency. Here spectral decomposition was performed on the raw online DC–200 Hz filtered data. For reasons cited above, statistical tests on the spectra between tFUS and sham conditions were conducted using nonparametric permutation statistics with a temporal cluster threshold of 13.4 ms and a $P < 0.025$, controlling for multiple comparisons as described by ref. 51. Data are presented parsed into the following frequency bands (Fig. 4): alpha band (7–12 Hz), beta band (13–30 Hz) and gamma band (30–55 Hz).

Examining the spatial specificity of tFUS on sensory-evoked brain activity. *Participants.* Eight volunteer participants (6 male, 2 female, aged 22–57 with a mean age of 28.8 ± 11.6 years) provided written informed consent to participate in the study. None of the volunteers reported any neurological impairment and were all self-reported as right-hand dominant.

Experimental setup. The set-up and approaches were identical to those described above. However, tFUS was projected from transducers placed at sites 1 cm anterior and 1 cm posterior to CP3 during MN stimulation trials. Both anterior and posterior sites were collected in the same session. Placement of the transducer (anterior versus posterior) as well as treatment condition (tFUS versus Sham) was pseudorandomly assigned among subjects such that either anterior or posterior placement was collected first in half of the subjects.

The influence of tFUS on two-point discrimination behavior. *Participants.* Twelve volunteer participants (5 male, 7 female, aged 23–57 with a mean age of 30.4 ± 10.4 years) provided written informed consent to participate in the study. None of the volunteers reported any neurological impairment and all were self-reported as right-hand dominant.

Experimental setup. Subjects were seated in a desk chair with their right arm resting on a tabletop with the pad of their index finger resting over a 1.3-cm hole through which stimuli were delivered. A total of nine pin (diameter = 200 μ m) separation distances were used including (0, 0.7, 1.0, 1.3, 1.6, 1.9, 2.2, 2.5, 2.8 mm). Each pin distance was randomly applied at a constant force of 1 N to the fingertip ten times during tFUS or sham treatment. After each stimulus, participants were required to report verbally whether they felt one or two pins. Before formal testing, participants were familiarized with the sensations produced by pins separated by 0 (one pin), 1.6 and 2.8 mm and informed after each stimulus to the fingertip whether the stimulus was one or two pins. Practice sessions of 10 trials of each pin distance (0, 1.6 and 2.8) were conducted. Formal testing began once participants achieved 80% (8/10) correct responses in response to stimulation using 0 mm and 2.8 mm pin distances. Participants were not aware of how many pin distances were used or the ratio of single to double pins during formal testing. Participants were not allowed to look at their fingers, but they were allowed to have their eyes open or closed. It was not possible for the participant to see the pins, as they were occluded from view under a table.

A custom-made motorized device that was controlled by custom-made software (LabVIEW, National Instruments, Austin, TX) was built to apply the pin to the fingertip. This allowed for precisely controlled force (1 N) and duration (250 ms) of the pins to the fingertip. The software also timed the onset of tFUS (500 ms duration) to occur 100 ms before the pin application to the fingertip. Participants underwent the sensory discrimination testing during both tFUS and sham treatment conditions in the same testing session. The order of sham or tFUS treatment was counterbalanced across subjects. The tFUS methods and parameters were identical to those reported earlier. Total collection time was approximately 1 h.

Statistical analysis. Signal detection theory was used to assess two-point discrimination thresholds as previously described⁵³. In this case, a two-response (one pin or two pin) design was used. Signal detection theory provides for the analysis of the two stages of information processing: (i) signal processing from sensory evidence and (ii) the decision whether the signal is present or not. Signal detection theory thus provides measures of participants' true sensitivity (d') and their bias for responding a certain way (c). To assess sensitivity, each participants' percentage correct at each pin distance was calculated. In instances where accuracy was 1 or 0, proportions were adjusted by $1/(2N)$ and $1/(1 - 2N)$, respectively, where N is the number of trials per condition. Data were z -score transformed and analyzed using two-response classifications and cumulative d' values as previously described⁵³. The detection threshold was chosen as $d' = 1$. Thus, this is the smallest pin distance that can be determined by a d' of 1. d' data were fitted using a third-degree polynomial. To assess threshold differences between tFUS and sham stimulation, the pin distance where each participant first achieved a d' prime > 1 was recorded for both tFUS and sham and subjected to a Wilcoxon rank sum test for statistical significance. To determine if responder bias contributes to the perceptual results, the criterion value c was calculated using the data from the one-pin and two-pin trials with the formula $c = 0.5[z(H) + z(FA)]$ (ref. 53), where z is the inverse of the normal cumulative distribution function, H is hit rate and FA is the false alarm rate. H was defined as responding one pin when one pin was present plus responding two pins when two pins were present. FA was defined as responding two pins when one pin was present. A criterion value of 0 reflects no bias for responding. Negative values indicate a tendency to report a stimulus when there is none (FA) and positive values the opposite. In this case, a positive value reflects a tendency toward saying two pins when there was only one and a negative value a tendency toward saying one pin when there were two. The parameter c was calculated for each subject for both the tFUS and sham session and subjected to a Wilcoxon rank-sum test for statistical significance. In addition, the percentage correct (hits/total trials) for the one-pin trials were quantified for both tFUS and sham conditions and statistical significance was assessed using a Wilcoxon sign-rank test.

The influence of tFUS on sensory discrimination behavior during frequency discrimination tasks. *Participants.* Twelve subjects (5 male, 7 female, aged 20–57 with a mean age of 31.8 ± 11.8 years) provided written informed consent to participate in the study. None of the volunteers reported any neurological impairment or neuropathic condition, and all were self-reported as right-hand dominant.

Experimental setup. The physical setup was similar to above. Subjects' right index finger rested on a 1.3-cm-diameter opening in which air puff stimuli were delivered. Air puff stimuli were generated using a Picospritzer III (Parker Instruments, Cleveland, OH) with a constant pressure of 14.5 p.s.i. delivered through a 1.88-mm-diameter aperture that contacted the volar surface of the index finger. This translated to a force of 0.3 N applied to the fingertip. A two-alternative forced choice method was employed in which the first stimulus was always a constant frequency of 100 Hz and the second stimulus was either the same frequency or higher. Participants were required to orally respond after cessation of the second stimulus "higher" if they thought the second stimulus was higher in frequency or "same" if they thought it was the same. The experimenter recorded the response on a computer. Ten frequencies were used from 100 Hz to 150 Hz in 5-Hz steps. The stimulus duration was 500 ms and the inter-stimulus interval was 500 ms. A total of 120 pairs of stimuli were delivered at an average inter-trial interval (ITI) of 6 s. A total of 40 catch trials (100 Hz–100 Hz) were randomly delivered throughout the test protocol. The ITI was not constant owing to varying response times of the participants.

The timing of stimuli was controlled by a custom-made program in written in LabVIEW (National Instruments, Austin, TX). The program also controlled the timing of tFUS such that it was delivered at the onset of the second air puff stimulus. Ultrasound waveform parameters were identical to those reported under “tFUS waveform” above. Before formal testing, participants were familiarized with the air puff stimuli at 100, 125 and 150 Hz. Practice sessions were conducted until participants achieved an 80% success rate on the maximally separated 100–150 Hz pair. Participants were not aware of how many frequency differences were used or the ratio of same to different frequencies. Participants were not allowed to look at their fingers, but they were allowed to have their eyes open or closed. Participants were provided with headphones that played white noise to block any auditory cues from the air puffer apparatus.

Statistical analysis. Signal detection theory was used to assess frequency discrimination thresholds, similarly to the method reported for two-point discrimination. Briefly, each volunteer’s percentage correct at each frequency difference was calculated. In instances where accuracy was 1 or 0, proportions were adjusted by $1/(2N)$ or $1/(1 - 2N)$, respectively, where N is the number of trials per condition. Data were z -score transformed and analyzed using two-response classification and cumulative d' . Detection threshold was chosen as $d' = 1$. Data were fitted using a third-degree polynomial. The frequency difference where each participant first achieved a cumulative $d' > 1$ was recorded for both tFUS and sham and subjected to a Wilcoxon rank-sum test for statistical

significance. In addition, the percentage correct (hits/total trials) for the same frequency trials was quantified for both tFUS and sham conditions and statistical significance was assessed using a Wilcoxon sign-rank test.

46. Windhoff, M., Opitz, A. & Thielscher, A. Electric field calculations in brain stimulation based on finite elements: an optimized processing pipeline for the generation and usage of accurate individual head models. *Hum. Brain Mapp.* **34**, 923–935 (2013).
47. Goss, S.A., Johnston, R.L. & Dunn, F. Comprehensive compilation of empirical ultrasonic properties of mammalian tissues. *J. Acoust. Soc. Am.* **64**, 423–457 (1978).
48. Legon, W., Rowlands, A., Opitz, A., Sato, T.F. & Tyler, W.J. Pulsed ultrasound differentially stimulates somatosensory circuits in humans as indicated by EEG and fMRI. *PLoS ONE* **7**, e51177 (2012).
49. Tufail, Y., Yoshihiro, A., Pati, S., Tauchmann, M.L. & Tyler, W.J. Ultrasonic neuromodulation by brain stimulation with transcranial ultrasound. *Nat. Protoc.* **6**, 1453–1470 (2011).
50. Delorme, A. & Makeig, S. EEGLAB: an open source toolbox for analysis of single-trial EEG dynamics including independent component analysis. *J. Neurosci. Methods* **134**, 9–21 (2004).
51. Maris, E. & Oostenveld, R. Nonparametric statistical testing of EEG- and MEG-data. *J. Neurosci. Methods* **164**, 177–190 (2007).
52. Makeig, S. Auditory event-related dynamics of the EEG spectrum and effects of exposure to tones. *Electroencephalogr. Clin. Neurophysiol.* **86**, 283–293 (1993).
53. Macmillan, N.A. & Creelman, C.D. *Detection Theory: A User's Guide* 2nd edn. (Erlbaum, 2005).